Graphene Oxide/Melamine/Ionic Liquid Membranes for Selective CO_2 Separation

Ahmad Arabi Shamsabadi*, Vahid Rad, and Masoud Soroush*

Department of Chemical and Biological Engineering, Drexel University, Philadelphia, PA 19104, USA

September 30, 2024

Revised Version

Submitted for Publication in Nano Trends

Keywords: Graphene Oxide, Functionalization, CO_2 Separation, Melamine, Ionic Liquids

*Corresponding authors: arabishamsabadi@gmail.com, soroushm@drexel.edu

Abstract

Highly permeable and selective membranes with long-term stability are needed to reduce operating and capital costs of industrial gas-separation units. In this study, we fabricate new membranes made of melamine (M)- and imidazolium-based ionic liquid (IL)-modified graphene oxide (GO) deposited on a porous support and buried with a polydimethylsiloxane (PDMS) layer. The CO_2/N_2 and CO_2/CH_4 selectivities of the composite membranes are respectively 65 % and 70 % higher than those of the membranes containing only the IL. This significant improvement in selectivity is attributed to synergic effects of nanochannels created by GO, fixed facilitated transport provided by the IL and numerous amine groups in the melamine structure, and the increased polarity of the membrane caused by the presence of the IL. The composite membrane has a CO_2 permeance of 47 GPU with a high CO_2/N_2 selectivity of 109 and a satisfactory CO_2/CH_4 selectivity of 39. The composite membrane maintains stable performance over a 60-hour operation, highlighting its long-term reliability. The outstanding performance, coupled with the ease of fabrication, underscores the potential of these composite membranes for practical and efficient CO_2 removal from both natural and flue gas streams in real-world applications.

Introduction

The increasing global demand for energy, chemicals, and water has led to a rise in CO_2 emissions, exacerbating the adverse environmental effects. Addressing the need to mitigate atmospheric CO_2 concentration has become a focal point in recent years. Membrane technology has emerged as a promising solution for CO_2-related challenges, owing to its inherent simplicity, energy efficiency, and cost-effectiveness [1-5]. However, to achieve a significant reduction in membrane-gas-separation costs, there is a critical requirement for the adoption of high-performance, thin, and stable membranes [4, 6-9].

Graphene oxide (GO) has attractive properties, including its hydrophilicity due to the presence of highly polar groups containing atomic oxygen (hydroxyl, epoxy, and carboxyl groups) on the surface and edges of GO, good dispersion in aqueous solutions, tuned microporosity, good stacking, beneficial modification, hydrogen-bonding and electrostatic forces, and high CO_2 affinity [10-12]. Because of these attractive properties, GO has been used as the main component or a dispersed phase in gas-separation membranes [10, 13-15]. For example, GO's good dispersion in aqueous solutions and excellent compatibility with polyether block amide (Pebax) copolymer led to the fabrication of mixed-matrix membranes with high sieving ability (CO_2/N_2 selectivity of 91) and surprisingly high stability (> 6000 min) [16]. However, the embedment of GO nanosheets into polymer matrices is bounded by challenges that are common in mixed-matrix membranes. Integrated GO films serving as the selective layer of gas separation membranes have been developed successfully [17]. Stacking and alignment of GO on porous substrates is an approach to fabricate ultra-thin membranes (<0.1 μm) [18]. Ultra-fast, long term-stable, and selective gas separation was achieved using the external force driven assembly approach [17]. External and internal forces were applied to give an orderly structure to GO laminates and to manipulate GO

passages to the sub-nanometer scale for faster transport of H_2 over CO_2. Highly permeable (CO_2 permeance of 650 GPU) and selective (CO_2/CH_4 of 75) GO-based membranes were synthesized by Wang et. al. [19]. The ultrathin GO membranes with high water contents were fabricated using borate as the crosslinker and facilitated transport carrier, to have a combination of engineered porosity, nanochannels, fixed facilitated transport for fast and favorable passage of CO_2 and blockage of other gases with a larger kinetic diameter such as CH_4 and N_2.

The functionalization of GO with amine groups increases the affinity toward CO_2 molecules and improves CO_2 uptake due to the so-called fixed facilitated transport [20-22]. Ionic liquids (ILs) have been found to be promising materials for facilitated transport of CO_2 molecules [23]. The use of ILs in gas-separation membranes has led to development of new approaches for CO_2 separation [24]. ILs comprising an acetate anion have a high tendency for CO_2 attraction [25]. In the case of imidazolium-based ILs, in addition to the formation of a complex between cation and carboxylic groups, the imidazolium groups interact with GO arene rings via π-π stacking [26, 27]. Karunakaran et al. [27] synthesized GO doped IL ultrathin membranes on a polymeric ultra-porous support coated with poly(1-trimethylsilyl-1-propyne) (PTMSP) as a protecting layer. The membranes exhibited CO_2 permeance of 37 GPU and CO_2/N_2 selectivity of 130. Despite the high gas permeability of PTMSP, the PTMSP membrane showed poor resistance to physical aging; the permeability of a 700 nm-PTMSP film significantly dropped in a 10-h operation [28]. The protecting layer should have very high gas permeability and excellent thin-film formability. Teflon AF and PTMSP have been used in laboratory studies, while polydimethylsiloxane (PDMS), a cross-linked rubbery polymer, has been employed in industrial applications [29]. Porous materials such as metal–organic frameworks (MOFs), covalent organic frameworks (COFs), and Zeolite-Y as protecting layers can be used as a protecting layer due to their high gas permeability.

In this research, we modify GO nanosheets with melamine in an aqueous medium and then interact the resulting solution (M-GO) with 1-ethyl-3-methylimidazolium acetate ([EMIM][Ac]) ionic liquid. We used GO sheets for fabricating functionalized membranes due to their excellent dispersion in water as well as the rich chemistry [30]. The excellent dispersion of GO in water is ascribed to the relatively high O/C ratio of GO and its hydrophilicity [31]. The epoxy, hydroxyl and carboxyl groups exist on the basal planes and edges of the sheets are beneficial for GO modification with melamine and interactions with the IL. We modified GO with melamine, because melamine provides CO_2 hydrophilic groups for the fixed facilitated transport. [EMIM][Ac] is a commercially available IL that is miscible with aqueous solutions. In addition, the imidazolium group in the structure of the IL provides high CO_2 solubility capacity, and the IL has excellent interaction with GO nanosheets [27]. We coated the M-GO-IL solution on PAN porous supports and buried the M-GO-IL layer with a PDMS layer. The performance of the prepared membranes for CO_2 separation from natural and flue gases is evaluated.

Experimental

Materials

PDMS (Sylgard® 184) including two parts was purchased from Dow Company. Polyacrylonitrile (PAN) was bought from Pfaltz & Bauer. Graphene oxide dispersed in water (4 mg/mL) was provided by Graphenea, Spain (Figure S1). 1-Ethyl-3-methylimidazolium acetate [EMIM][Ac] ionic liquid (>95%), was procured from IOLITEC. Melamine was bought from Alfa Aesar, and dimethylformamide (DMF) and n-hexane were obtained from BTC. N_2 (99.999 %), CH_4 (99.99%), and bon-dry CO_2 (99.9%) were supplied from Air gas. In all experiments, demineralized (DI) water was used.

Modification of GO with melamine

GO sheets were modified with melamine (M) to obtain M-GO sheets. 5 mL of GO suspension (4 mg/mL) was diluted to obtain 20 mL suspension with 1 mg/mL GO concentration. After 10 min sonication, the pH was raised to 9 with a 0.1 M sodium carbonate solution followed by 30 min sonication to obtain completely exfoliated and well dispersed GO. Next, 42 mg (0.33 mmol) melamine was added to the mixture, and the suspension was sonicated for 2 h. During the sonication, the bath temperature was maintained at 22°C. The M-GO solid was obtained via centrifugation washed with water several times to remove unreacted melamine and dried under vacuum.

Membrane preparation

Firstly, a 20 wt% IL stock solution was prepared by stirring 20 g of the IL and 80 g water for 1 h. Four M-GO-IL suspensions with different concentrations were then prepared by adding the IL solution to the M-GO suspensions, and the pH of the solution was increased to 11 by adding a 1 M NaOH solution and then sonicating for 60 min.

Substrates of the nanocomposite membranes were synthesized from PAN because it possesses satisfactory thermal, chemical and mechanical stability even without any additives and post-treatment [32]. Hydrophilicity and wettability provide well dispersion and coating of aqueous solutions on the support surface [33, 34]. Porous supports were fabricated using the so-called phase inversion method [35] by dissolving PAN powder in DMF solvent overnight at 35 °C to obtain a 12 wt% homogenous solution. After removing all gas bubbles, the PAN solution was cast using a film applicator and immersed in a water bath at 21°C. After 30 min the PAN support was removed from the water bath and stored in the fresh DI water for complete solvent exchange. The support

was then wetted with methanol before use to increase its hydrophilicity. **Figure S2** (**Supporting Information, SI**) shows top surface and cross-sectional SEM images of the PAN substrate.

Twice dip coating was employed for putting M-GO-IL on the sealed PAN supports followed by removing excess solution and drying under fume hood for 2 days. We prepared a 1wt% Sylgard 184 solution by dissolving a 10:1 ratio of the PDMS component to the hardener one in n-hexane. The membranes were then submerged entirely in the Sylgard solution to protect the impregnated IL impregnated from leaching. The fabricated membranes were dried at ambient temperature for 48 h. A schematic of the membrane fabrication steps is presented in **Figure 1**.

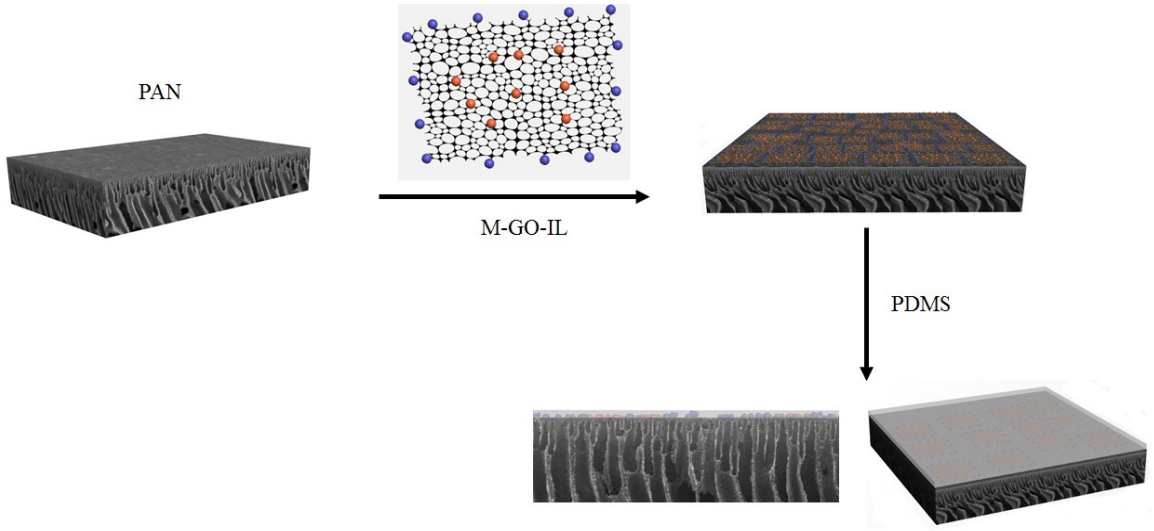

Figure 1. Schematic representation of the membrane fabrication steps.

Results and discussion

We modified GO sheets with melamine according to the nucleophilic reaction of the $–NH_2$ functionality of melamine and the epoxy group of GO (**Figure 2**) [36]. The presence of melamine alters the interlayer spacing and interactions between GO sheets, as verified by X-ray diffraction (XRD) analysis which is discussed later. In addition, the numerous amine groups of melamine can

strongly affect the performance of fabricated membranes via the so-called fixed facilitated transport [37]. The modified GO sheets were treated with the [EMIM] [Ac] IL. A complex was formed after the exchange of cation from the IL and the carboxylic groups present on the edges of GO sheets (**Figure 2**). The GO modification and the treatment with the IL were performed in aqueous media which are crucial for manufacturability and sustainability of the fabrication process. The use of water as the coating solvent improves the fabrication process safety, facilitates waste management, and enables straight forward and cost-effective roll-to-roll coating in large-scale production.

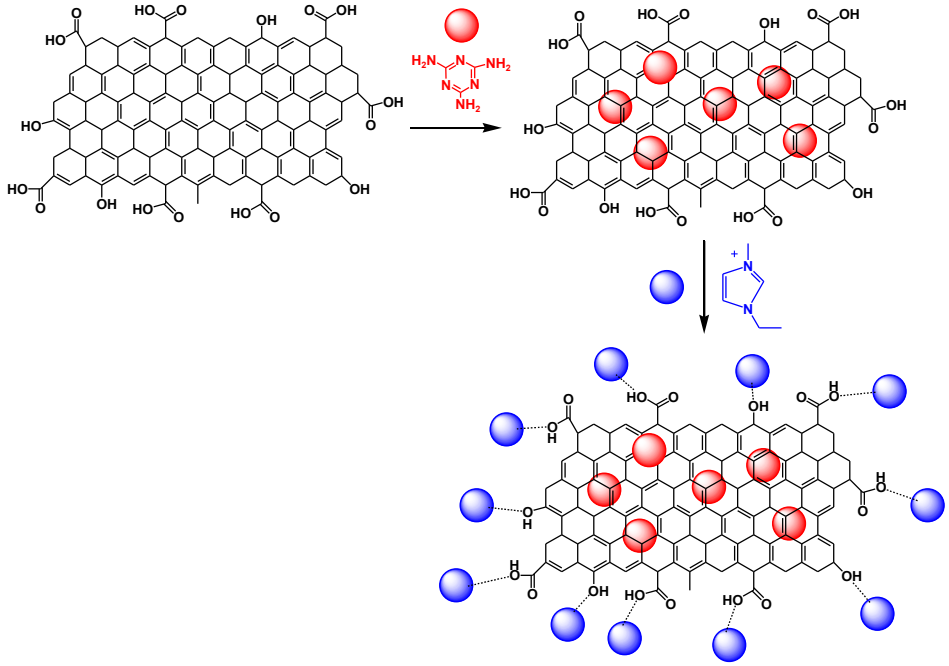

Figure 2. Modification of GO with melamine and ionic liquid complexation.

The modification of GO with melamine and complexation of the IL with the modified GO were analyzed using Fourier-transform infrared spectroscopy (FTIR), XRD, X-ray photoelectron spectroscopy (XPS), Raman spectroscopy, scanning electron microscopy (SEM), and transmission electron microscopy (TEM). **Figures 3a and 3b** show FTIR spectra of GO, melamine (M),

[EMIM] [Ac], M-GO, and M-GO-IL. The peaks related to oxygen-containing functional groups were observed in FTIR spectrum of the pristine GO. The peaks at 1733, 1361, 1243, and 1051 cm^{-1} are attributed to C=O, O–H deformation, C–O–C (epoxy), and C–OH stretching vibrations, respectively. In melamine FTIR spectrum, the primary amine peaks appeared at 3469, 3411, 3313, and 3120 cm^{-1}, while 1629, 1533,1436, and 813 cm^{-1} represent the stretching modes of the triazinyl [38]. Upon the GO modification with melamine, the peak intensity of the epoxy group in melamine–GO was largely reduced as compared to that of GO, which may be ascribed to the reaction of the epoxy groups of GO and amine groups of melamine to form either amides or alkylammonium via the ring-opening amination of epoxides [36]. The presence of melamine peaks in the M-GO with some shifts verifies the successful surface modification of GO. Finally, after the complexation of the modified GO with IL, main vibrational stretching modes of the IL can be observed in the FTIR spectrum of M-GO-IL (**Figure 3b**). The surface modification of GO was further characterized using XPS analysis. High resolution C 1s spectrum of GO, indicates all expected C=C and various oxygen-containing functionalities of GO (**Figure 3c**) [39]. The C 1s spectrum of the modified GO with melamine (M-GO) displays all the GO peaks and an extra peak at 285.3 eV, which can be related to the C–N/C=N (**Figure 3d**). Furthermore, XPS elemental analysis indicates 6.67% of nitrogen element for the modified GO, which is absent in the GO as expected (**Table 1, SI**). The presence of nitrogen and the C–N bond in the M-GO verifies the grafting of melamine on GO. Moreover, the reduction of C–O–C bond content (**Table 2, SI**) after modification also corroborates the reaction of melamine with the epoxy groups on the GO surface. XRD pattern of GO, M, M-GO-, and M-GO-IL were collected to identify the change in crystallinity of GO upon modification and the complexation with the IL (**Figure 3e**). The strong diffraction peak at about 9.6° is known as the (002) plane of GO. The main characteristic peaks of

melamine at approximately 12.8, 14.3, and 26.2° are attributed to (–101), (–111), and (–301) diffraction planes, respectively (**Figure 3e**) [40]. The reduced 2θ of the main peaks of melamine and GO, and increased intensity of (–101), (–111) diffraction planes, together with the decreased intensity of the (–301) diffraction plane further confirm the modification of GO with melamine (**Figure 3e**). The decreased 2θ values of the (002) plane of GO in the nanocomposite indicate larger d-spacing between the GO nanosheets upon modifications with melamine and the IL. The downward shifts of all diffraction peaks of M-GO-IL compared to M-GO imply the complexation of the IL with M-GO sheet (**Figure 3e**) [27]. Raman spectra of GO, M-GO, M-GO-IL are presented in **Figure 3f.** In the GO spectrum, the carbon characteristic peaks at 1601.7 cm^{-1} and 1341.9 cm^{-1} correspond to the first-order G and D peaks, respectively. Melamine modification changed the G and D peaks of GO to lower wavenumbers 1596.9 cm^{-1} and 1337.6 cm^{-1}. The Raman spectrum of the complex of the modified GO and [EMIM][Ac] shows shifted carbon characteristic peaks to 1594.7 cm^{-1} and 1339.5 cm^{-1}. In addition, this spectrum has slightly broader peaks than the GO and M-GO spectra, corroborating the interactions between the IL and the modified GO composite.

The morphology of the nanomaterials was studied using SEM and TEM analyses. As can be seen in the TEM image of GO **(Figure 4a)**, a typical silk-like morphology with several was observed. After the modification, melamine was distributed uniformly on the GO **(Figure 4b)**. The addition of the IL to the modified GO sheets did not change the morphology of M-GO **(Figure 4c)**. The SEM image of GO **(Figure 4d)** shows that the morphology of GO is model folded. Using melamine as a modifying agent resulted in a less accumulated morphology for the M-GO hybrid composite (**Figure 4e**). Furthermore, melamine crystals are distinguishable in the SEM image (**Figure 4e**). The less packed M-GO sheets are adhered together upon interaction with the IL which are extremely different from initial shapes of GO and M-GO sheets (**Figure 4f**).

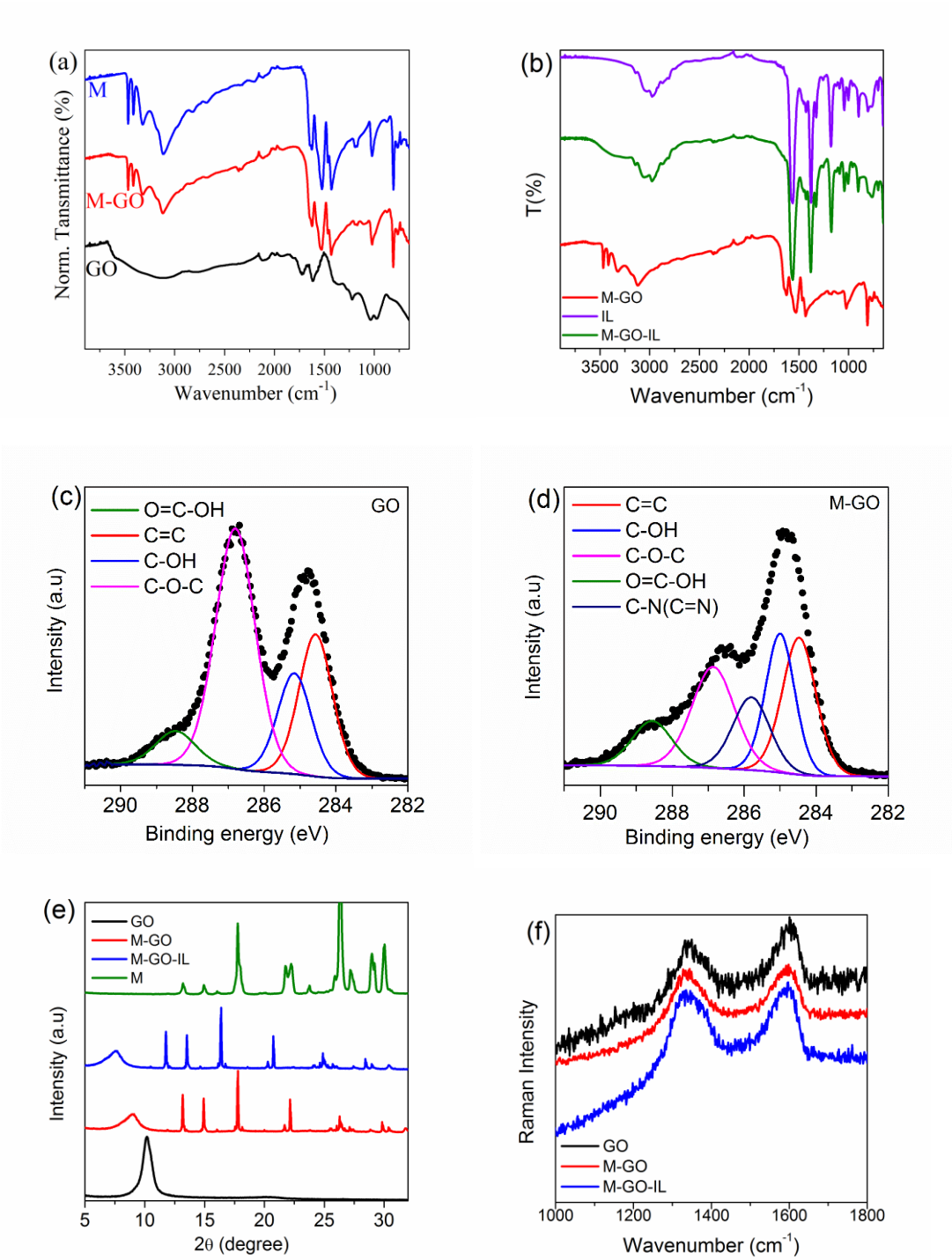

Figure 3. (a), (b) FTIR spectra of GO, M-GO, and M-GO-IL, (c) high resolution C1s spectrum of GO, (d) high resolution C1s spectrum of M-GO, (e) XRD patterns of GO, M-GO, and M-GO-IL, and (f) Raman spectra of GO, M-GO, and M-GO-IL.

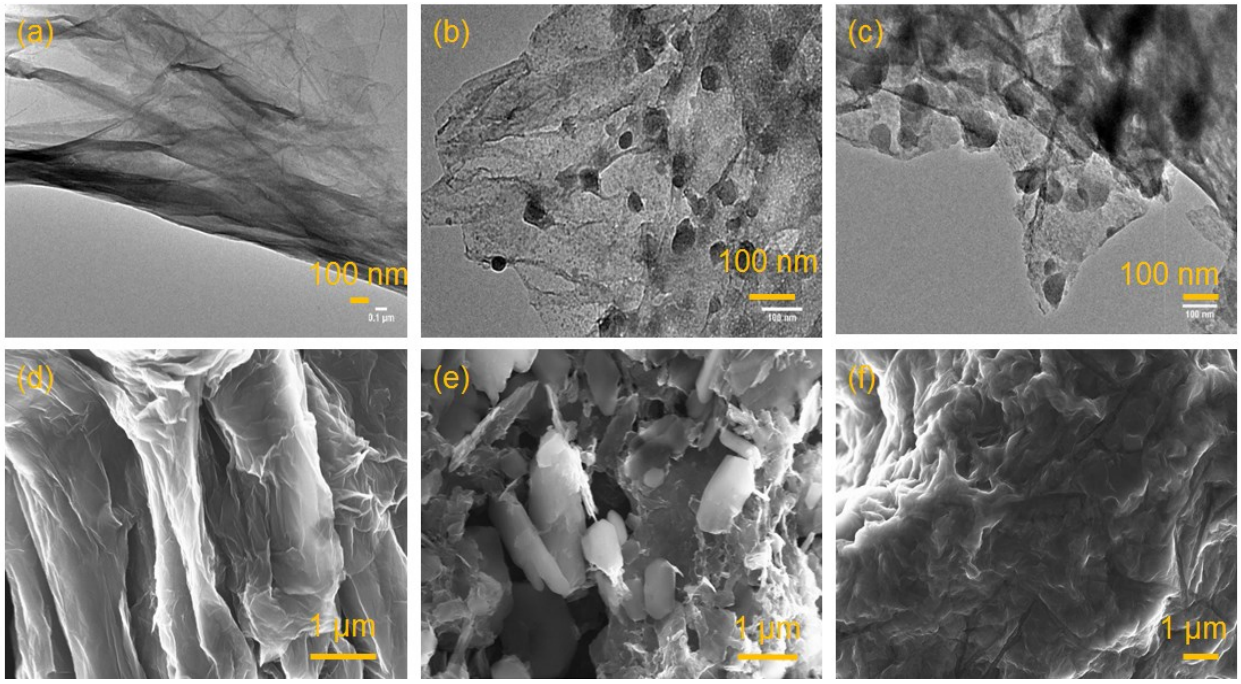

Figure 4. TEM micrographs of (a) GO, (b) M-GO, and (c) M-GO-IL, and SEM images of (d) GO, (e) M-GO, and (f) M-GO-IL.

We used sonication during the surface modification of GO with melamine and the complexation of the modified GO with the IL. Sonication of GO sheets can break the sheets into smaller pieces [41]. We conducted dynamic light scattering (DLS) tests at pH 5 for the three samples to measure particle sizes [42]. An average size of 2 µm with a broad distribution was observed for GO (**Figure S3a, SI**). In the case of M-GO, the average particle size decreased to 317 nm with a narrow distribution that can be attributed to decreased GO size upon sonication and de-stacking of the GO sheets after reaction with melamine (**Figure S3a, SI**). In fact, melamine molecules are voluminous enough to de-bundle GO sheets and create enough steric hindrance to prevent re-stacking of the GO sheets. Upon complexation of the IL with the modified GO the average particle size increased from 317 nm to 560 nm (**Figure S3a, SI**). Here, the IL plays the

role of an organic salt that reduces electrostatic repulsion forces experienced by adjacent M-GO sheets resulting in an increase in the average particle size ultraviolet-visible (UV-Vis) spectra of GO, M-GO, M-GO-IL are displayed in **Figure S3b, SI**. The shoulder at 300 nm and the maximum at 212 nm are the characteristic peaks of GO. Comparing UV-Vis spectra of GO and M-GO reveals a blue shift of the maximum absorption from 212 nm to around 204 nm, also the shoulder at 300 nm disappeared after surface modification (**Figure S3b, SI)**. It can be concluded that melamine groups are incorporated into GO sheets successfully. After the addition of the IL to M-GO, the M-GO-IL spectrum demonstrated a red shift to 212 nm, further confirming the complexation of the IL with the modified GO (**Figure S3b, SI)**.

Figure 5 shows the surface (left) and cross-sectional (right) images of the PAN/IL-M-GO/PDMS membrane. The GO sheets cover most parts of the PAN support creating more tortuous pathways for gas transport. The cross-sectional image indicates a 400-480 nm thick PDMS protecting layer on the top of the nanocomposite membrane. The PDMS protecting layer is well attached to the support.

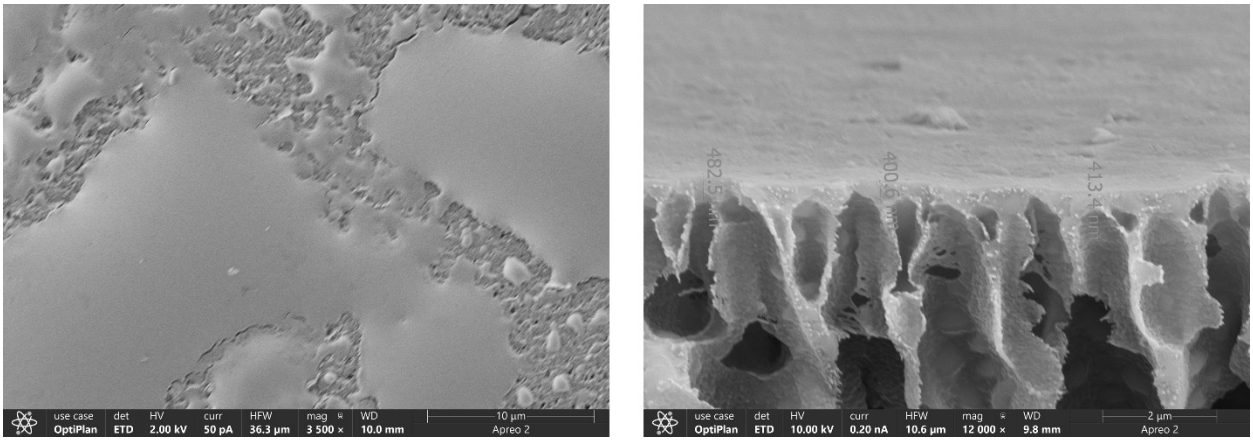

Figure 5. Surface (left) and cross-sectional (right) SEM images of PAN/IL-M-GO/PDMS membrane.

Gas permeation tests

Gas permeation tests for all membranes were conducted using a home-made set up working with the pressure constant method (**Figure S4, SI)** at 1 bar and 22 °C using pure gases in order of N_2, CH_4 and CO_2. High permeance rate and no sieving ability of the PAN support revealed no resistance against gas passage through the support and thereby Knudsen as the governing mechanism. For selective membranes, the fastest transport belonged to CO_2 compared to lower permeance for CH_4 and N_2 permeance (**Figure 6a**). Significant lower CO_2 permeance 53 GPU of IL impregnated PDMS/PAN membrane compared to PDMS membranes together with higher CO_2/N_2 selectivity indicates successful impregnation of IL molecules in the pores of the PAN substrate [43]. A previous study shows that, for supported [EMIM][Ac] membranes using different supports, satisfactory CO_2/N_2 selectivity were achieved in the range of 30–35 [44]. However, the IL-PAN membrane coated by PDMS in this study exhibited almost 1.9 times higher CO_2/N_2 selectivity compared to the supported [EMIM][Ac] membrane with the best selectivity (35) (**Figure 6b**). The observed difference could have been caused by the viscous gas flow through unfilled pores with IL and different pore sizes of the supports. Capability of PDMS to seal unfilled pores [45] and decrease the viscous gas flow resulted in enhanced CO_2/N_2 selectivity. Compared to PTMSP/IL/PAN membranes [27], the PDMS/IL/PAN membranes demonstrated lower CO_2/N_2 and CO_2/CH_4 selectivities, but higher CO_2 permeance. The lower gas selectivity can be due to the better sealing of the support pores with PTMSP than PDMS (the non-crosslinked polymer versus the crosslinked polymer, respectively) and/or differences in supports.

To further increase CO_2 selectivity and stability of the IL-based membrane, the IL was combined with the M-GO composite. The influence of the M-GO concentration on the performance of IL-based membrane was investigated (**Figures 6a and 6b**). Despite the presence

of numerous amine groups in the modified GO sheets, a continuous reduction of permeance was observed for CO_2 upon the incorporation of the hybrid sheets (**Figure 6a)**. This can be attributed to stacking modified GO sheets on top of the support pores filled by the IL during the membrane fabrication [27]. In addition, adding up to 0.012 wt% hybrid composite sheets, resulted in decrease in N_2 and CH_4 permeances (**Figure 6a)**.

Compared to the IL membrane, the hybrid composite membrane comprising 0.012 wt% of the modified GO flakes resulted in a 65 % increase in CO_2/N_2 selectivity to 109 and a 70% increase in CO_2/CH_4 selectivity to 39 with just 12% decline in the CO_2 permeance (**Figures 6a and 6b**). The significant decrease in N_2 and CH_4 permeances can be ascribed to the restricted gas paths caused by the stacked modified GO. Longer gas-pathway sieving nanochannels provided by GO sheets with synergetic effect of fixed facilitated transport were responsible for the excellent improvement of CO_2 selectivities. Further increases in the GO concentration to 0.05 wt% had no considerable effect on N_2 and CH_4 transport but decreased the CO_2 permeance. The results are consistent with selectivity enhancement of membranes upon GO addition [27, 46]. The performance of the PAN/IL/PDMS and PAN/M-GO-IL/PDMS membranes was compared to the CO_2/N_2 upper bound of supported liquid membranes (**Figure 7a**). Transcending the upper bound with ultrathin IL-AC membranes reveals that ILs are promising materials with extraordinary performance for CO_2 removal from flue gas streams. Synergetic effects endowed by GO nanochannels, fixed facilitated transport, and PDMS as the sealing and protecting layer led to surpassing the trade-off curve with our membranes.

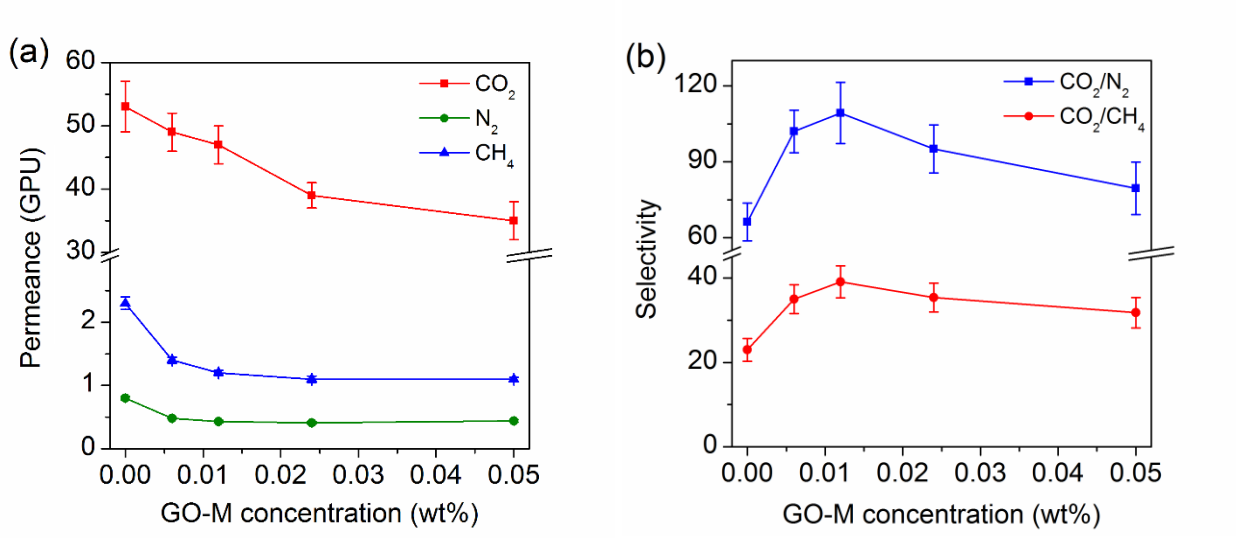

Figure 6. Effect of the modified GO (M-GO) concentration on (a) gas permeance and (b) CO_2/N_2 and CO_2/CH_4 selectivities of IL-based membranes tested at 1 bar.

Long term stability is crucial for the industrial use of membranes especially. For IL-based membranes this also includes mechanical and configurational stability. The decay of transport properties increases the capital and operating costs and lower profit margins. We used a continuous gas permeation test to evaluate the stability of the most selective membrane over 60 h. **Figures 7a and 7b** show the CO_2 permeance, CO_2/N_2 selectivity, and CO_2/CH_4 selectivity changes during 60 h. No considerable fluctuation was observed for gases transport properties. We did not observe any leaching issue verified by stable performance within 60 h. Furthermore, no defect was found after the stability test indicating excellent mechanical and configurational stability of the hybrid composite membrane. Excellent steady performance validates the synergic effects of M-GO-IL complex and strong interaction between amine groups and CO_2 molecules with no saturation [47]. In addition, exposing the most selective membrane to oxygen for 28 days upon its storage at ambient conditions did not compromise its transport properties, highlighting the potential of the PDMS protecting layer in preventing oxygen related degradation. The long-term stability together

with the ease of fabrication and excellent performance of the composite membranes indicates the potential of these membranes for industrial-scale removal of CO_2 from natural and flue gas streams.

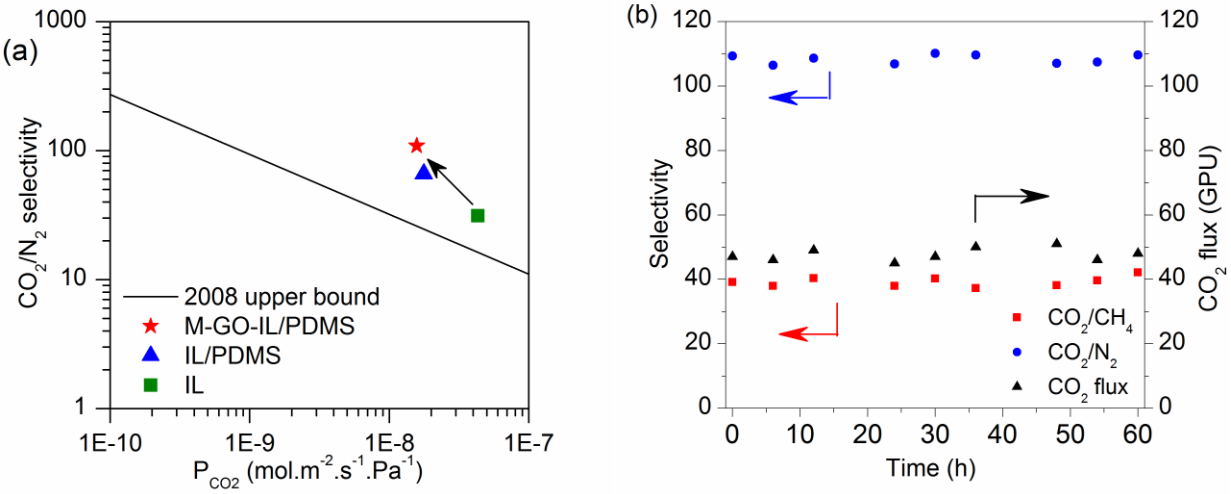

Figure 7. (a) Comparison of CO_2/N_2 separation performance of the membrane at 1 bar and 22 °C with the IL upper bound (IL data are from Jonathan Albo and Toshinori Tsuru [44]), and (b) CO_2 permeance, CO_2/N_2 and CO_2/CH_4 selectivities at 1 bar and 22 °C during 60 h.

Conclusions

In conclusion, this study has successfully addressed the pressing need for advanced membranes in CO_2 separation by employing a novel fabrication approach. The modification of graphene oxide (GO) with melamine, combined with the integration of [EMIM][Ac] ionic liquid (IL), resulted in the creation of CO_2 selective membranes. The critical enhancement of CO_2 selectivity was achieved through the strategic sealing of unfilled IL pores using polydimethylsiloxane (PDMS). Additionally, the incorporation of stacked GO/melamine sheets increased tortuosity and fixed facilitated transport, which in turn led to 65% and 70% improvement in CO_2/N_2 and CO_2/CH_4 selectivities, respectively, compared to those of membranes containing only the IL. This strategy

can be applied to other two-dimensional materials that are modifiable with melamine, to produce composite membranes. It can also be used to produce highly stable colloidal solutions with ILs.

Remarkably, the performance of the hybrid composite membranes surpassed the upper limits set by the IL, demonstrating their exceptional efficacy in CO_2 separation. The scalability of the fabrication method enhances the practical viability of these membranes for large-scale applications. The demonstrated high selectivity and outstanding stability of the composite membranes position them as promising candidates for addressing the challenges associated with CO_2 emissions in diverse industrial processes.

In summary, this research contributes valuable insights into the development of advanced membrane materials, offering a potential solution for mitigating environmental impact and advancing the efficiency of industrial gas separation processes. The findings underscore the significance of this approach in the broader context of sustainable technologies and underline the potential for real-world applications in CO_2 capture and separation.

References

1. Shamsabadi, A.A., et al., *A New Pentiptycene-Based Dianhydride and Its High-Free-Volume Polymer for Carbon Dioxide Removal.* ChemSusChem, 2018. **11**(2): p. 472-482.
2. Shamsabadi, A.A., et al., *Next generation polymers of intrinsic microporosity with tunable moieties for ultrahigh permeation and precise molecular CO2 separation.* Progress in Energy and Combustion Science, 2021. **84**: p. 100903.
3. Seidi, F., et al., *Biopolymer-based membranes from polysaccharides for CO2 separation: a review.* Environmental Chemistry Letters, 2022. **20**(2): p. 1083-1128.
4. Theodorakopoulos, G.V., et al., *Green chemistry-based fabrication of hollow fiber and flat sheet polyimide membranes for CO2/CH4 separation.* Journal of Membrane Science Letters, 2023. **3**(2): p. 100057.
5. Chen, K.K., et al., *Enhancing membrane performance for CO2 capture from flue gas with ultrahigh MW polyvinylamine.* Journal of Membrane Science, 2021. **628**: p. 119215.
6. Chang, C.-K., et al., *Conformational-change-induced selectivity enhancement of CAU-10-PDC membrane for H2/CH4 and CO2/CH4 separation.* Journal of Membrane Science Letters, 2021. **1**(1): p. 100005.
7. Shamsabadi, A.A., et al., *Pushing rubbery polymer membranes to be economic for CO2 separation: embedment with Ti3C2T x MXene nanosheets.* ACS Applied Materials & Interfaces, 2019. **12**(3): p. 3984-3992.
8. Zhang, S., et al., *Negative charge confined amine carriers within the nanowire network for stable and efficient membrane carbon capture.* Advanced Functional Materials, 2020. **30**(30): p. 2002804.
9. Yang, Y., et al., *A commercial-size prototype of countercurrent spiral-wound membrane module for flue gas CO2 capture.* Journal of Membrane Science, 2024: p. 122520.
10. Liu, G., W. Jin, and N. Xu, *Graphene-based membranes.* Chemical Society Reviews, 2015. **44**(15): p. 5016-5030.
11. Kim, H.W., et al., *High-performance CO 2-philic graphene oxide membranes under wet-conditions.* Chemical Communications, 2014. **50**(88): p. 13563-13566.
12. Ghouri, Z.K., et al., *Strong Improvement of Permeability and Rejection Performance of Graphene Oxide Membrane by Engineered Interlayer Spacing.* Journal of Membrane Science Letters, 2023: p. 100065.
13. Dong, G., et al., *Enhanced CO2/N2 separation by porous reduced graphene oxide/Pebax mixed matrix membranes.* Journal of Membrane Science, 2016. **520**: p. 860-868.
14. Najafi, M., et al., *Polysulfone membranes incorporated with reduced graphene oxide nanoparticles for enhanced Olefin/Paraffin separation.* ChemistrySelect, 2020. **5**(12): p. 3675-3681.
15. Zhou, F., et al., *Printed graphene oxide-based membranes for gas separation and carbon capture.* Chemical Engineering Journal, 2022. **430**: p. 132942.
16. Shen, J., et al., *Membranes with fast and selective gas-transport channels of laminar graphene oxide for efficient CO2 capture.* Angewandte Chemie, 2015. **127**(2): p. 588-592.
17. Shen, J., et al., *Subnanometer two-dimensional graphene oxide channels for ultrafast gas sieving.* ACS nano, 2016. **10**(3): p. 3398-3409.
18. Mi, B., *Graphene oxide membranes for ionic and molecular sieving.* Science, 2014. **343**(6172): p. 740-742.
19. Wang, S., et al., *A highly permeable graphene oxide membrane with fast and selective transport nanochannels for efficient carbon capture.* Energy & Environmental Science, 2016. **9**(10): p. 3107-3112.

20. Hong, S.-M., S.H. Kim, and K.B. Lee, *Adsorption of carbon dioxide on 3-aminopropyl-triethoxysilane modified graphite oxide.* Energy & Fuels, 2013. **27**(6): p. 3358-3363.
21. Dong, G., et al., *Graphene oxide nanosheets based novel facilitated transport membranes for efficient CO2 capture.* Industrial & Engineering Chemistry Research, 2016. **55**(18): p. 5403-5414.
22. Saedi, S., et al., *Fixed facilitated transport of CO2 through integrally-skinned asymmetric polyethersulfone membrane using a novel synthesized Poly (acrylonitrile-co-N, N-Dimethylaminopropyl acrylamide).* Chemical Engineering Journal, 2014. **236**: p. 263-273.
23. Fam, W., et al., *Gelled graphene oxide–ionic liquid composite membranes with enriched ionic liquid surfaces for improved CO2 separation.* ACS applied materials & interfaces, 2018. **10**(8): p. 7389-7400.
24. Dai, Z., et al., *Combination of ionic liquids with membrane technology: A new approach for CO2 separation.* Journal of Membrane Science, 2016. **497**: p. 1-20.
25. Santos, E., J. Albo, and A. Irabien, *Acetate based supported ionic liquid membranes (SILMs) for CO2 separation: Influence of the temperature.* Journal of membrane science, 2014. **452**: p. 277-283.
26. Yan, W., et al., *Rapid and effective functionalization of graphene oxide by ionic liquid.* Journal of nanoscience and nanotechnology, 2012. **12**(3): p. 2270-2277.
27. Karunakaran, M., et al., *Graphene oxide doped ionic liquid ultrathin composite membranes for efficient CO 2 capture.* Journal of Materials Chemistry A, 2017. **5**(2): p. 649-656.
28. Tiwari, R.R., et al., *Gas permeation in thin films of "high free-volume" glassy perfluoropolymers: Part I. Physical aging.* Polymer, 2014. **55**(22): p. 5788-5800.
29. Zhang, G. and H. Lin, *Indispensable gutter layers in thin-film composite membranes for carbon capture.* Green Energy & Environment, 2023.
30. Firouzjaei, M.D., et al., *Exploiting synergetic effects of graphene oxide and a silver-based metal–organic framework to enhance antifouling and anti-biofouling properties of thin-film nanocomposite membranes.* ACS applied materials & interfaces, 2018. **10**(49): p. 42967-42978.
31. Guan, K., et al., *Spray-evaporation assembled graphene oxide membranes for selective hydrogen transport.* Separation and Purification Technology, 2017. **174**: p. 126-135.
32. Scharnagl, N. and H. Buschatz, *Polyacrylonitrile (PAN) membranes for ultra-and microfiltration.* Desalination, 2001. **139**(1-3): p. 191-198.
33. Marchetti, P., M. Mechelhoff, and A.G. Livingston, *Tunable-porosity membranes from discrete nanoparticles.* Scientific reports, 2015. **5**(1): p. 17353.
34. Shamsabadi, A.A., et al., *Efficient CO 2-removal using novel mixed-matrix membranes with modified TiO 2 nanoparticles.* Journal of Materials Chemistry A, 2017. **5**(8): p. 4011-4025.
35. Saedi, S., S.S. Madaeni, and A.A. Shamsabadi, *PDMS coated asymmetric PES membrane for natural gas sweetening: effect of preparation and operating parameters on performance.* The Canadian Journal of Chemical Engineering, 2014. **92**(5): p. 892-904.
36. Gowthaman, N., M.A. Raj, and S.A. John, *Nitrogen-doped graphene as a robust scaffold for the homogeneous deposition of copper nanostructures: A nonenzymatic disposable glucose sensor.* ACS Sustainable Chemistry & Engineering, 2017. **5**(2): p. 1648-1658.
37. Saedi, S., et al., *Synthesis and application of a novel Amino-Starch derivative as a new polymeric additive for fixed facilitated transport of carbon dioxide through an asymmetric polyethersulfone (PES) membrane.* International Journal of Greenhouse Gas Control, 2013. **19**: p. 126-137.
38. Wang, D., et al., *Preparation and property analysis of melamine formaldehyde foam.* Adv. Mater. Phys. Chem, 2012. **2**(4): p. 63-67.
39. Firouzjaei, M.D., et al., *A novel nanocomposite with superior antibacterial activity: a silver-based metal organic framework embellished with graphene oxide.* Advanced Materials Interfaces, 2018. **5**(11): p. 1701365.

40. Lu, H., et al., *Influence of the Crystal Structure of Melamine Trimetaphosphate 2D Supramolecules on the Properties of Polyamide 6.* ACS Applied Materials & Interfaces, 2023. **15**(9): p. 12393-12402.
41. Perreault, F., et al., *Antimicrobial properties of graphene oxide nanosheets: why size matters.* ACS nano, 2015. **9**(7): p. 7226-7236.
42. Amaro-Gahete, J., et al., *A comparative study of particle size distribution of graphene nanosheets synthesized by an ultrasound-assisted method.* Nanomaterials, 2019. **9**(2): p. 152.
43. Li, P., H.Z. Chen, and T.-S. Chung, *The effects of substrate characteristics and pre-wetting agents on PAN–PDMS composite hollow fiber membranes for CO2/N2 and O2/N2 separation.* Journal of Membrane Science, 2013. **434**: p. 18-25.
44. Albo, J. and T. Tsuru, *Thin ionic liquid membranes based on inorganic supports with different pore sizes.* Industrial & Engineering Chemistry Research, 2014. **53**(19): p. 8045-8056.
45. Kargari, A., A.A. Shamsabadi, and M.B. Babaheidari, *Influence of coating conditions on the H2 separation performance from H2/CH4 gas mixtures by the PDMS/PEI composite membrane.* International Journal of Hydrogen Energy, 2014. **39**(12): p. 6588-6597.
46. Chae, I.S., et al., *The platform effect of graphene oxide on CO2 transport on copper nanocomposites in ionic liquids.* Chemical Engineering Journal, 2014. **251**: p. 343-347.
47. Sadeghi, M., et al., *Engineering the dispersion of nanoparticles in polyurethane membranes to control membrane physical and transport properties.* Chemical Engineering Science, 2018. **192**: p. 688-698.